Available online at www.sciencedirect.com
SCIENCE DIRECT®
Astroparticle Physics 23 (2005) 526–534
Astroparticle Physics
www.elsevier.com/locate/astropart

The atmospheric neutrino flux below 100 MeV: The FLUKA results

G. Battistoni [a,*], A. Ferrari [b,1], T. Montaruli [c,2], P.R. Sala [a]

[a] INFN, via Celoria 16, 20133 Milano, Italy
[b] CERN, Geneva, Switzerland
[c] University of Wisconsin, Madison, WI, USA

Received 4 February 2005; received in revised form 23 March 2005; accepted 23 March 2005
Available online 13 April 2005

Abstract

We present here the FLUKA results on the atmospheric neutrino flux below 100 MeV, down to 10 MeV. Atmospheric neutrinos in this energy range can be detected by high resolution liquid argon detectors. Below ~50 MeV, the interaction of these neutrinos are an important background in the searches of relic neutrinos from SuperNovae.

PACS: 14.60.Lm; 97.60.Bw; 95.85.Ry

Keywords: Supernova relic neutrinos; Atmospheric neutrinos

1. Introduction

When a massive star ($\gtrsim 8M_{\odot}$) collapses as a Type II Supernova (SNII), ~99% of its energy is emitted as $\sim 10^{53}$ erg neutrinos. The neutrinos from all SNII occurred in the Universe should constitute an isotropic cosmological flux of core-collapse SN Relic Neutrinos (SRN in the following). Recently Super-Kamiokande [1] and KamLAND [2] published their results on SRNs. SNO [3] presented a preliminary measurement of the solar $\bar{\nu}_e$ flux that could easily be adapted to this measurement. Besides SN physics, the SRN measurement can be used to constrain neutrino decay models since this process could substantially alter expected fluxes [4,5].

The main background sources for SRN are solar, atmospheric and possibly reactor neutrinos in the relevant energy range of $\lesssim 50$ MeV. Solar neutrinos

* Corresponding author. Tel.: +39 250317307; fax: +39 250317624.
E-mail address: giuseppe.battistoni@mi.infn.it (G. Battistoni).
[1] On leave of absence from INFN, Milano, Italy.
[2] On leave of absence from Universitá di Bari, Dipartimento di Fisica, Bari, Italy.

0927-6505/$ - see front matter
doi:10.1016/j.astropartphys.2005.03.006

overwhelm the SRN flux at energies lower than the ^8B and *hep* flux end-points at $\lesssim$20 MeV. At higher energies ($\gtrsim$ 40 MeV) the atmospheric ν background is the most dangerous contribution. The $\bar{\nu}_e$ atmospheric ν flux has the same signature than the SRN signal. Moreover, ν_μ quasi-elastic scattering interactions in water Čerenkov detectors, like Super-Kamiokande, produce an unmeasurable background due to the decay products of invisible muons, that are below the threshold for Čerenkov light emission ($E_{kin} < 50$ MeV). It has been pointed out that a possible window of observation of the SRN signal is between 20 and 30 MeV.

As a first attempt to explore the SRN region, Super-Kamiokande and Kamland made use of the calculation in Ref. [6] to estimate the atmospheric ν background. Also the HKKM calculation [7] was used in Ref. [8].

Beyond the interest concerning an improved evaluation of the atmospheric background in SRN search, atmospheric neutrinos of very low energy are important of the design study of large Liquid Argon Time Projection Chamber detectors. The ICARUS experiment [9] proposes this technology and the detector is going to be installed in the Gran Sasso laboratory in the next. It will offer the possibility of detecting atmospheric neutrinos with a lower energy threshold with respect to the Čerenkov case. At very low energy this technique is mainly sensitive to ν_e of energies $\gtrsim$ 5 MeV interacting through charged current interactions, though it is also sensitive to all neutrino flavor neutral current interactions, but with smaller probability due to the different cross sections.

For all these motivations we present here the FLUKA results on atmospheric neutrino fluxes down to 10 MeV.

In the following we summarize the essential elements of the low energy atmospheric neutrino calculations and discuss the main sources of uncertainties. We provide here flux tables calculated for the Gran Sasso laboratory and Super-Kamiokande sites. It must be intended that in our simulation the difference in site is only due to the geomagnetic cutoff. We have not yet introduced any attempt to take into account the effect of the local atmosphere and of the ground profile (mountain shape, elevation, etc.). We are aware that these details may account for a few percent systematics in the determination of low energy atmospheric neutrino fluxes.

2. Atmospheric neutrino flux calculation at low energy

The FLUKA atmospheric neutrino flux has been proposed mostly to satisfy the needs of second generation experiments, and of ICARUS in particular, for a highly detailed calculation. As a matter of fact, the FLUKA Monte Carlo provides a high accuracy transport model and a set of particle production models which are maintained at a very high level of accuracy from the point of view of both theoretical principles and experimental constraints from accelerator data.

The first interesting result from the FLUKA set up was the enhancement in the horizontal region of the sub-GeV atmospheric neutrino flux [10], which was soon reproduced by other groups. The full description of the calculation has been reported in [11], where fluxes are given between 100 MeV and about 50 GeV. The extension of the calculation above 50 GeV up to 10 TeV was presented in [12]. Uncertainties on this calculation have been discussed in [11] and in [13]. The atmospheric neutrino calculation is also being checked by producing predictions of other measurable fluxes of secondary particles in the atmosphere, such as muons. After the comparison with the CAPRICE94 [14] data, that we consider as a very important validation step of the general features of FLUKA results on atmospheric neutrinos, we are presently comparing with the muon fluxes measured by the BESS experiments [15].

The FLUKA neutrino calculation were originally performed using a minimum energy cutoff 10 MeV, although until now we had never derived results for the region below 100 MeV. Details on our flux calculation can be found in the references quoted above. Here we recall the baseline choices of our calculation:

(1) The primary spectrum in the region of kinetic energy per nucleon relevant for this topic (between 0.5 GeV and 100 GeV) is

constrained by the results of AMS [16] and BESS [17] for proton and helium. We are aware of the CAPRICE data [18], which exhibit a normalization about 25% lower. This is a relevant source of uncertainty.
(2) We are considering the superposition model in FLUKA, namely the primary flux is converted into an all-nucleon flux.[3]
(3) We use a spherical representation of the earth and the surrounding atmosphere up to 70 km a.s.l.
(4) We are using the average USA standard atmosphere over the whole earth surface. The atmosphere is layered in 100 shells with a density scaling according to the chosen profile as a function of height.
(5) The geomagnetic cutoff is applied by means of the back-tracing technique using the IGRF model.
(6) We use the solar modulation model in [19].

3. Results and discussion

The shape of the neutrino flux without including oscillation effects in the low energy region is presented in Fig. 1. Here the angle integrated flux at the Kamioka site is shown for solar cycle average for $\nu_e + \bar{\nu}_e$ and $\nu_\mu + \bar{\nu}_\mu$ from 10 MeV up to 1 GeV. In the same figures the Bartol group calculations [6] are also shown for comparison. We have not enough information to give an exact explanation of the difference between our estimate of the flux with respect to that of [6], however we know that there are at least three main ingredients which can contribute: the primary spectrum, the particle production model, and the 3-dimensional spherical geometrical representation of earth and atmosphere vs. the flat geometry. We believe that the first two elements are the most important causes at the origin of the disagreement. In particular, the primary spectrum described in Section 2, for a given interaction model, is known to produce more neutrinos at low energy with respect to previous choices, as shown in Ref. [20]. In Appendix A we provide tables of angle integrated fluxes calculated for the average solar cycle at the sites of the Gran Sasso laboratory and of Super-Kamiokande. We give both electron and muon neutrino fluxes for neutrinos and anti-neutrinos. Providing all these fluxes allows interested readers to account for 3-family neutrino oscillations and matter effects that at these energies should be considered for a proper event rate estimate in a detector.

The structures visible in the shape of the fluxes are due to processes which are not relevant for neutrinos exceeding 100 MeV: the decay at rest of pions and muons which stop arriving at the end of their range. The π^+ 2-body decay originates the monochromatic spike in the ν_μ flux at about 30 MeV. FLUKA accounts also for the $\pi^+ \to e^+\nu_e$ decay but being the branching ratio of 1.2×10^{-4} the effect is invisible on the ν_e flux. Instead π^- are all captured and undergo nuclear interaction. The shoulder around 53 MeV in both ν_e and ν_μ fluxes is due to the decay at rest of muons. FLUKA takes into account a Z-dependent capture probability for μ^-. After capture, μ^- still produces neutrinos through scattering with one or more nucleons. In the FLUKA model the following processes are considered:

$$\mu^- + p \to n + \nu_\mu, \tag{1}$$

$$\mu^- + p + p(n) \to n + p(n) + \nu_\mu. \tag{2}$$

The relative contribution of the process in Eq. (2) is chosen in such a way to reproduce the measured neutron spectrum for elements where experimental data exist. The dynamics is modeled according to the phase space. None of these processes gives monochromatic neutrinos, also because of the Fermi motion in the nucleus. The upper energy of these ν_μ's is however around 100 MeV, with a spread extending up to significantly lower values. Therefore there are no easily observable features in the flux shape associated to these capture processes.

[3] At present FLUKA does include models for nucleus–nucleus collisions but we are not yet using it for atmospheric neutrino productions.

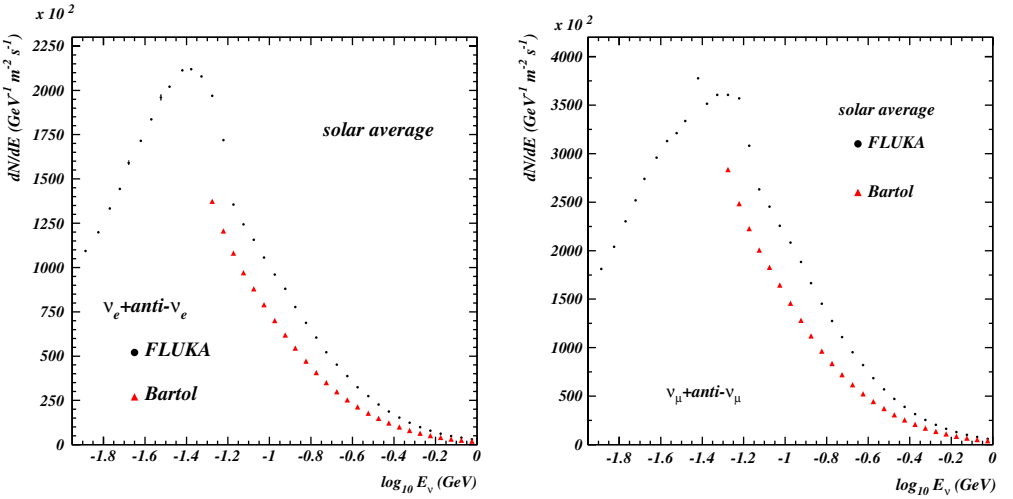

Fig. 1. $\nu_e + \bar{\nu}_e$ (left) and $\nu_\mu + \bar{\nu}_\mu$ (right) angle integrated differential flux for solar average at the Super-Kamiokande site not including oscillations: dots are for FLUKA and triangles for the Bartol group calculation [6].

Table 1
Fraction of each neutrino flavor with energy below 100 MeV

	ν_μ	$\bar{\nu}_\mu$	ν_e	$\bar{\nu}_e$
Stopping μ decay	0.078	0.070	0.124	0.148
μ decay in flight	0.378	0.470	0.876	0.852
Stopping π decay	0.003	0.007	0.00002	$\sim$0
π decay in flight	0.541	0.453	0.00003	0.00005
K decay in flight	0.0005	0.0003	0.0007	0.0006
Total fraction of each flavor	0.329	0.338	0.183	0.150

Total fraction and contribution by the different production channels are given.

Table 1 summarized the calculated fraction of different channels producing neutrinos in the energy range below 100 MeV. The differences between ν and $\bar{\nu}$ reflect the different abundances of π^+ and π^- produced in p-nucleus collisions and the capture probabilities of π's and μ's.

In Fig. 2 we show the distribution of the vertical production height of all neutrinos of energy less or equal to 100 MeV, together with the average flight distance as a function of the cosine of the zenith angle. The flight distance difference between ν_e and ν_μ is not larger than 5% for neutrinos coming from above. This small difference is not surprising: as stated above, for this energy selection almost one half of muon neutrinos are produced in muon decay, as electron neutrinos. Furthermore, for $E_\nu < 100$ MeV, the difference between the average vertical production height (between 18 and 20 km above sea level) of ν_μ and $\bar{\nu}_\mu$ coming from π and that of neutrinos coming from muon decay turns out to be less than 1.5 km. At higher energy, when parent muon energy is also higher, the difference in vertical production height increases, with ν_e and $\bar{\nu}_e$ being generated in average at a significantly lower altitude. For example, considering multi-GeV neutrinos around the vertical, the difference in flight path approaches 20%.

In Fig. 3 we show the distribution of energy/nucleon of the primaries which contribute to neutrinos from 10 MeV to 100 MeV for a low geomagnetic cutoff site. This distribution is not qualitatively different from that of the whole sub-GeV region. The median value is almost correspondent to the energy value where in FLUKA there is a transition in the hadronic interaction model: below 5 GeV the generalized intranuclear cascade and pre-equilibrium model (called PEANUT) is used, while above this value we switch to the Dual Parton Model. The comparison with

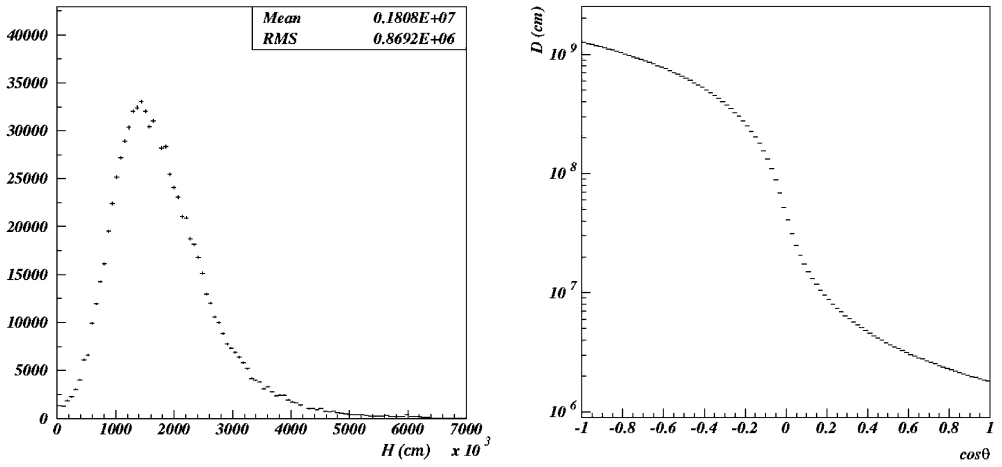

Fig. 2. Distribution of the vertical production height of all neutrinos below 100 MeV (left). Average flight distance of all neutrinos versus the cosine of the zenith angle (right).

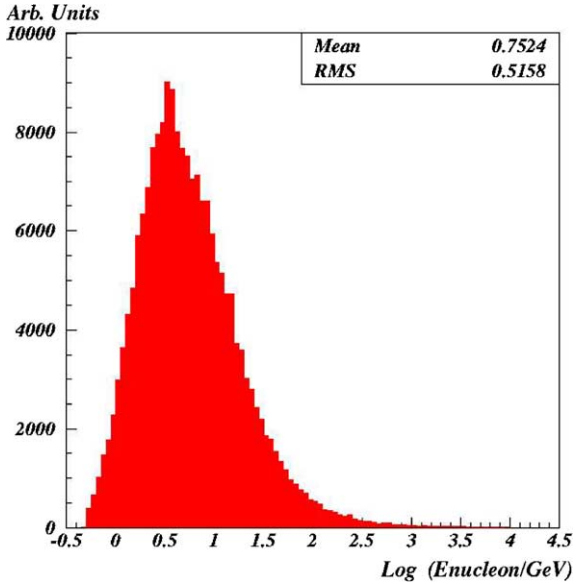

Fig. 3. Distribution of energy/nucleon of the primary nucleons which contribute to atmospheric neutrinos from 10 MeV to 100 MeV.

accelerator results presented in [11] allows us to estimate a systematic error on particle production in FLUKA in the whole energy region between pion threshold and 100 GeV which is not larger than 15%. The data coming from dedicated experiments like HARP [21] will hopefully provide a further benchmark of the relevant energy region for the problem considered here.

4. Conclusions

The results presented here can be reliably used for background evaluation in SRN searches and can be used to estimate the sensitivity of future Megaton Čerenkov and liquid Ar multi-kton detectors in the search for relic ν's.

The atmospheric neutrinos in the very low energy region between 10 and 100 MeV are produced in the same kinematic region denominated as "sub-GeV", following the Super-Kamiokande classification. There, the most important uncertainties are still related to the knowledge of the primary spectrum and in part to the hadronic interaction models. These are much more important than other details like those associated to atmosphere model and local ground shape. Our estimate is that the overall uncertainty on the absolute value of these fluxes is not larger than 25% and it is dominated by the uncertainty on the primary spectrum. The flavor ratio is well under control, since these low energy neutrinos are produced in a regime where the decay chain $\pi \to \mu \to \nu$ is fully effective, and the K contribution to neutrino production is practically negligible here.

Comparisons of the event rates [22] using the atmospheric ν flux in [8,1,23], show that previous calculations underestimated by up to 40% for $E_{e^+} \lesssim 30$ MeV the atmospheric neutrino background as compared to what is predicted by this work.

Within the ICARUS collaboration, these results have been already used to evaluate the possibility of detecting SRNs [24].

Acknowledgment

We would like to thank A. Mirizzi, E. Lisi, D. Montanino for having stimulated this work.

Appendix A. Tables of neutrino fluxes

See Tables 2–5.

Table 2
Differential fluxes in energy for no oscillations for ν_μ and $\bar{\nu}_\mu$ ($\mathrm{GeV}^{-1}\,\mathrm{m}^{-2}\,\mathrm{s}^{-1}$) for solar average at the site of Super-Kamiokande

E_ν (GeV)	dN_{ν_μ}/dE ($\mathrm{GeV}^{-1}\,\mathrm{m}^{-2}\,\mathrm{s}^{-1}$)	$dN_{\bar{\nu}_\mu}/dE$ ($\mathrm{GeV}^{-1}\,\mathrm{m}^{-2}\,\mathrm{s}^{-1}$)
0.013	0.114E+06 ± 0.994E+03	0.116E+06 ± 0.656E+03
0.015	0.124E+06 ± 0.710E+03	0.128E+06 ± 0.792E+03
0.017	0.138E+06 ± 0.788E+03	0.136E+06 ± 0.522E+03
0.019	0.146E+06 ± 0.596E+03	0.150E+06 ± 0.490E+03
0.021	0.155E+06 ± 0.644E+03	0.158E+06 ± 0.600E+03
0.024	0.159E+06 ± 0.540E+03	0.162E+06 ± 0.407E+03
0.027	0.164E+06 ± 0.591E+03	0.170E+06 ± 0.500E+03
0.030	0.181E+06 ± 0.576E+03	0.196E+06 ± 0.774E+03
0.033	0.174E+06 ± 0.420E+03	0.177E+06 ± 0.495E+03
0.038	0.179E+06 ± 0.829E+03	0.182E+06 ± 0.505E+03
0.042	0.178E+06 ± 0.537E+03	0.183E+06 ± 0.537E+03
0.047	0.176E+06 ± 0.269E+03	0.181E+06 ± 0.437E+03
0.053	0.153E+06 ± 0.395E+03	0.155E+06 ± 0.334E+03
0.060	0.131E+06 ± 0.237E+03	0.132E+06 ± 0.372E+03
0.067	0.123E+06 ± 0.635E+03	0.123E+06 ± 0.415E+03
0.075	0.114E+06 ± 0.310E+03	0.112E+06 ± 0.218E+03
0.084	0.107E+06 ± 0.152E+03	0.101E+06 ± 0.220E+03
0.094	0.963E+05 ± 0.218E+03	0.921E+05 ± 0.239E+03
0.106	0.842E+05 ± 0.203E+03	0.822E+05 ± 0.187E+03
0.119	0.727E+05 ± 0.145E+03	0.725E+05 ± 0.110E+03
0.133	0.635E+05 ± 0.187E+03	0.640E+05 ± 0.158E+03
0.150	0.552E+05 ± 0.125E+03	0.556E+05 ± 0.112E+03
0.168	0.477E+05 ± 0.878E+02	0.476E+05 ± 0.942E+02
0.188	0.412E+05 ± 0.245E+03	0.408E+05 ± 0.102E+03
0.211	0.344E+05 ± 0.827E+02	0.341E+05 ± 0.880E+02
0.237	0.284E+05 ± 0.558E+02	0.286E+05 ± 0.610E+02
0.266	0.236E+05 ± 0.762E+02	0.235E+05 ± 0.516E+02
0.299	0.196E+05 ± 0.412E+02	0.193E+05 ± 0.336E+02
0.335	0.158E+05 ± 0.395E+02	0.157E+05 ± 0.363E+02
0.376	0.128E+05 ± 0.348E+02	0.126E+05 ± 0.238E+02
0.422	0.103E+05 ± 0.276E+02	0.102E+05 ± 0.268E+02
0.473	0.820E+04 ± 0.162E+02	0.815E+04 ± 0.216E+02
0.531	0.649E+04 ± 0.121E+02	0.648E+04 ± 0.309E+02
0.596	0.515E+04 ± 0.128E+02	0.502E+04 ± 0.115E+02
0.668	0.398E+04 ± 0.109E+02	0.394E+04 ± 0.117E+02
0.750	0.313E+04 ± 0.150E+02	0.303E+04 ± 0.935E+01
0.841	0.241E+04 ± 0.626E+01	0.233E+04 ± 0.921E+02
0.944	0.182E+04 ± 0.548E+01	0.179E+04 ± 0.428E+01

The energy value is at bin center for 40 equally spaced $\log_{10} E$ bins between 10 and 10^3 MeV.

Table 3
Differential fluxes in energy for no oscillations for ν_e and $\bar{\nu}_e$ ($GeV^{-1}\ m^{-2}\ s^{-1}$) for solar average at the site of Super-Kamiokande

E_ν (GeV)	dN_{ν_e}/dE ($GeV^{-1}\ m^{-2}\ s^{-1}$)	$dN_{\bar{\nu}_e}/dE$ ($GeV^{-1}\ m^{-2}\ s^{-1}$)
0.013	0.696E+05 ± 0.695E+03	0.637E+05 ± 0.377E+03
0.015	0.746E+05 ± 0.435E+03	0.697E+05 ± 0.453E+03
0.017	0.797E+05 ± 0.384E+03	0.795E+05 ± 0.114E+04
0.019	0.874E+05 ± 0.419E+03	0.842E+05 ± 0.461E+03
0.021	0.942E+05 ± 0.429E+03	0.894E+05 ± 0.355E+03
0.024	0.101E+06 ± 0.149E+04	0.950E+05 ± 0.878E+03
0.027	0.103E+06 ± 0.364E+03	0.993E+05 ± 0.535E+03
0.030	0.109E+06 ± 0.690E+03	0.103E+06 ± 0.371E+03
0.033	0.108E+06 ± 0.361E+03	0.104E+06 ± 0.470E+03
0.038	0.107E+06 ± 0.354E+03	0.101E+06 ± 0.330E+03
0.042	0.101E+06 ± 0.376E+03	0.961E+05 ± 0.288E+03
0.047	0.885E+05 ± 0.341E+03	0.835E+05 ± 0.291E+03
0.053	0.696E+05 ± 0.202E+03	0.659E+05 ± 0.204E+03
0.060	0.644E+05 ± 0.200E+03	0.600E+05 ± 0.260E+03
0.067	0.593E+05 ± 0.198E+03	0.564E+05 ± 0.212E+03
0.075	0.543E+05 ± 0.145E+03	0.514E+05 ± 0.137E+03
0.084	0.497E+05 ± 0.105E+03	0.463E+05 ± 0.177E+03
0.094	0.451E+05 ± 0.124E+03	0.430E+05 ± 0.480E+03
0.106	0.406E+05 ± 0.118E+03	0.372E+05 ± 0.121E+03
0.119	0.358E+05 ± 0.972E+02	0.329E+05 ± 0.875E+02
0.133	0.317E+05 ± 0.199E+03	0.288E+05 ± 0.951E+02
0.150	0.273E+05 ± 0.680E+02	0.249E+05 ± 0.777E+02
0.168	0.239E+05 ± 0.549E+02	0.213E+05 ± 0.648E+02
0.188	0.204E+05 ± 0.104E+03	0.183E+05 ± 0.440E+02
0.211	0.170E+05 ± 0.457E+02	0.154E+05 ± 0.412E+02
0.237	0.145E+05 ± 0.951E+02	0.129E+05 ± 0.445E+02
0.266	0.120E+05 ± 0.338E+02	0.106E+05 ± 0.315E+02
0.299	0.996E+04 ± 0.293E+02	0.880E+04 ± 0.251E+02
0.335	0.811E+04 ± 0.276E+02	0.713E+04 ± 0.151E+02
0.376	0.662E+04 ± 0.172E+02	0.575E+04 ± 0.248E+02
0.422	0.527E+04 ± 0.124E+02	0.460E+04 ± 0.192E+02
0.473	0.423E+04 ± 0.114E+02	0.368E+04 ± 0.119E+02
0.531	0.337E+04 ± 0.313E+02	0.288E+04 ± 0.111E+02
0.596	0.266E+04 ± 0.790E+01	0.228E+04 ± 0.698E+01
0.668	0.209E+04 ± 0.693E+01	0.187E+04 ± 0.414E+02
0.750	0.162E+04 ± 0.537E+01	0.137E+04 ± 0.431E+01
0.841	0.124E+04 ± 0.424E+01	0.106E+04 ± 0.485E+01
0.944	0.950E+03 ± 0.339E+01	0.800E+03 ± 0.249E+01

The energy value is at bin center for 40 equally spaced $\log_{10} E$ bins between 10 and 10^3 MeV.

Table 4
Differential fluxes in energy for no oscillations for ν_μ and $\bar{\nu}_\mu$ ($GeV^{-1}\ m^{-2}\ s^{-1}$) for solar average at the site of the Gran Sasso laboratory

E_ν (GeV)	dN_{ν_μ}/dE ($GeV^{-1}\ m^{-2}\ s^{-1}$)	$dN_{\bar{\nu}_\mu}/dE$ ($GeV^{-1}\ m^{-2}\ s^{-1}$)
0.013	0.174E+06 ± 0.114E+04	0.173E+06 ± 0.789E+03
0.015	0.190E+06 ± 0.114E+04	0.194E+06 ± 0.115E+04
0.017	0.211E+06 ± 0.998E+03	0.211E+06 ± 0.263E+04
0.019	0.220E+06 ± 0.794E+03	0.226E+06 ± 0.801E+03
0.021	0.235E+06 ± 0.898E+03	0.241E+06 ± 0.103E+04
0.024	0.243E+06 ± 0.940E+03	0.247E+06 ± 0.733E+03
0.027	0.248E+06 ± 0.736E+03	0.260E+06 ± 0.895E+03
0.030	0.275E+06 ± 0.108E+04	0.299E+06 ± 0.985E+03

Table 4 (*continued*)

E_ν (GeV)	dN_{ν_μ}/dE (GeV^{-1} m^{-2} s^{-1})	$dN_{\bar{\nu}_\mu}/dE$ (GeV^{-1} m^{-2} s^{-1})
0.033	0.263E+06 ± 0.610E+03	0.269E+06 ± 0.527E+03
0.038	0.270E+06 ± 0.105E+04	0.276E+06 ± 0.789E+03
0.042	0.269E+06 ± 0.730E+03	0.279E+06 ± 0.928E+03
0.047	0.266E+06 ± 0.475E+03	0.276E+06 ± 0.743E+03
0.053	0.232E+06 ± 0.605E+03	0.233E+06 ± 0.476E+03
0.060	0.197E+06 ± 0.422E+03	0.199E+06 ± 0.604E+03
0.067	0.182E+06 ± 0.723E+03	0.184E+06 ± 0.531E+03
0.075	0.169E+06 ± 0.450E+03	0.166E+06 ± 0.275E+03
0.084	0.157E+06 ± 0.283E+03	0.149E+06 ± 0.308E+03
0.094	0.141E+06 ± 0.299E+03	0.137E+06 ± 0.465E+03
0.106	0.123E+06 ± 0.310E+03	0.119E+06 ± 0.258E+03
0.119	0.105E+06 ± 0.230E+03	0.105E+06 ± 0.205E+03
0.133	0.912E+05 ± 0.240E+03	0.915E+05 ± 0.219E+03
0.150	0.785E+05 ± 0.152E+03	0.790E+05 ± 0.156E+03
0.168	0.672E+05 ± 0.134E+03	0.675E+05 ± 0.162E+03
0.188	0.575E+05 ± 0.265E+03	0.572E+05 ± 0.146E+03
0.211	0.476E+05 ± 0.107E+03	0.474E+05 ± 0.118E+03
0.237	0.391E+05 ± 0.831E+02	0.394E+05 ± 0.855E+02
0.266	0.325E+05 ± 0.150E+03	0.321E+05 ± 0.741E+02
0.299	0.262E+05 ± 0.442E+02	0.260E+05 ± 0.408E+02
0.335	0.212E+05 ± 0.630E+02	0.209E+05 ± 0.447E+02
0.376	0.169E+05 ± 0.451E+02	0.166E+05 ± 0.335E+02
0.422	0.134E+05 ± 0.322E+02	0.133E+05 ± 0.358E+02
0.473	0.105E+05 ± 0.209E+02	0.105E+05 ± 0.290E+02
0.531	0.825E+04 ± 0.173E+02	0.821E+04 ± 0.312E+02
0.596	0.640E+04 ± 0.147E+02	0.629E+04 ± 0.147E+02
0.668	0.490E+04 ± 0.145E+02	0.488E+04 ± 0.162E+02
0.750	0.378E+04 ± 0.156E+02	0.371E+04 ± 0.117E+02
0.841	0.287E+04 ± 0.716E+01	0.281E+04 ± 0.102E+02
0.944	0.214E+04 ± 0.727E+01	0.211E+04 ± 0.497E+01

The energy value is at bin center for 40 equally spaced $\log_{10}E$ bins between 10 and 10^3 MeV.

Table 5
Differential fluxes in energy for no oscillations for ν_e and $\bar{\nu}_e$ (GeV^{-1} m^{-2} s^{-1}) for solar average at the site of the Gran Sasso laboratory

E_ν (GeV)	dN_{ν_e}/dE (GeV^{-1} m^{-2} s^{-1})	$dN_{\bar{\nu}_e}/dE$ (GeV^{-1} m^{-2} s^{-1})
0.013	0.105E+06 ± 0.893E+03	0.964E+05 ± 0.650E+03
0.015	0.114E+06 ± 0.632E+03	0.105E+06 ± 0.698E+03
0.017	0.121E+06 ± 0.681E+03	0.117E+06 ± 0.114E+04
0.019	0.133E+06 ± 0.967E+03	0.124E+06 ± 0.584E+03
0.021	0.140E+06 ± 0.620E+03	0.133E+06 ± 0.473E+03
0.024	0.152E+06 ± 0.152E+04	0.142E+06 ± 0.938E+03
0.027	0.158E+06 ± 0.751E+03	0.147E+06 ± 0.590E+03
0.030	0.165E+06 ± 0.763E+03	0.153E+06 ± 0.510E+03
0.033	0.164E+06 ± 0.483E+03	0.153E+06 ± 0.664E+03
0.038	0.161E+06 ± 0.455E+03	0.153E+06 ± 0.740E+03
0.042	0.153E+06 ± 0.503E+03	0.143E+06 ± 0.414E+03
0.047	0.134E+06 ± 0.419E+03	0.125E+06 ± 0.593E+03
0.053	0.105E+06 ± 0.286E+03	0.978E+05 ± 0.347E+03
0.060	0.960E+05 ± 0.315E+03	0.886E+05 ± 0.365E+03
0.067	0.885E+05 ± 0.223E+03	0.823E+05 ± 0.324E+03

(*continued on next page*)

Table 5 (*continued*)

E_ν (GeV)	dN_{ν_e}/dE (GeV^{-1} m^{-2} s^{-1})	$dN_{\bar{\nu}_e}/dE$ (GeV^{-1} m^{-2} s^{-1})
0.075	0.808E+05 ± 0.213E+03	0.748E+05 ± 0.182E+03
0.084	0.735E+05 ± 0.248E+03	0.670E+05 ± 0.190E+03
0.094	0.671E+05 ± 0.325E+03	0.612E+05 ± 0.486E+03
0.106	0.595E+05 ± 0.172E+03	0.531E+05 ± 0.162E+03
0.119	0.519E+05 ± 0.139E+03	0.466E+05 ± 0.106E+03
0.133	0.457E+05 ± 0.228E+03	0.406E+05 ± 0.127E+03
0.150	0.394E+05 ± 0.150E+03	0.347E+05 ± 0.909E+02
0.168	0.340E+05 ± 0.912E+02	0.295E+05 ± 0.872E+02
0.188	0.292E+05 ± 0.109E+03	0.253E+05 ± 0.971E+02
0.211	0.241E+05 ± 0.746E+02	0.211E+05 ± 0.851E+02
0.237	0.203E+05 ± 0.103E+03	0.176E+05 ± 0.632E+02
0.266	0.168E+05 ± 0.561E+02	0.143E+05 ± 0.437E+02
0.299	0.140E+05 ± 0.202E+03	0.118E+05 ± 0.365E+02
0.335	0.110E+05 ± 0.412E+02	0.943E+04 ± 0.225E+02
0.376	0.894E+04 ± 0.267E+02	0.758E+04 ± 0.264E+02
0.422	0.706E+04 ± 0.218E+02	0.595E+04 ± 0.226E+02
0.473	0.557E+04 ± 0.154E+02	0.467E+04 ± 0.185E+02
0.531	0.445E+04 ± 0.341E+02	0.364E+04 ± 0.132E+02
0.596	0.344E+04 ± 0.130E+02	0.284E+04 ± 0.906E+01
0.668	0.267E+04 ± 0.915E+01	0.226E+04 ± 0.413E+02
0.750	0.211E+04 ± 0.233E+02	0.168E+04 ± 0.819E+01
0.841	0.153E+04 ± 0.596E+01	0.127E+04 ± 0.716E+01
0.944	0.116E+04 ± 0.391E+01	0.938E+03 ± 0.380E+01

The energy value is at bin center for 40 equally spaced $\log_{10} E$ bins between 10 and 10^3 MeV.

References

[1] M. Malek et al. Super-Kamiokande Collaboration, Phys. Rev. Lett. 90 (2003) 061101.
[2] K. Eguchi et al. KamLAND Collaboration, Phys. Rev. Lett. 92 (2004) 071301.
[3] T. Kutter for the SNO Collaboration, Antineutrino Search at the Sudbury Neutrino Observatory, in: Proceedings of 28th International Cosmic ray Conference (ICRC 2003), July 31–August 7 2003, Tsukuba, Japan, p. 1233.
[4] S. Ando, Phys. Lett. B 570 (2003) 11.
[5] G.L. Fogli, E. Lisi, A. Mirizzi, D. Montanino, Phys. Rev. D 70 (2004) 013001, e-print: hep-ph/0401227.
[6] T.K. Gaisser, T. Stanev, G. Barr, Phys. Rev. D 39 (1989) 3532.
[7] M. Honda, T. Kajita, K. Kasahara, S. Midorikawa, Phys. Rev. D 52 (1995) 4985.
[8] M. Malek, PhD thesis. Available from: http://www.sk.icrr.u-tokyo.ac.jp/doc/sk/pub/malek-thesis.pdf.
[9] S. Amerio et al. (ICARUS Collaboration), Nucl. Instrum. Methods A 527 (2004) 329, and references therein.
[10] G. Battistoni et al., Astropart. Phys. 12 (2000) 315.
[11] G. Battistoni, A. Ferrari, T. Montaruli, P.R. Sala, Astropart. Phys. 19 (2003) 269, Erratum, Astropart. Phys. 19 (2003) 291.
[12] G. Battistoni, A. Ferrari, T. Montaruli, P.R. Sala, High energy extension of the FLUKA atmospheric neutrino flux, in Proceedings of 28th International Cosmic Ray Conference (ICRC 2003), Tsukuba, Japan, 31 July–7 August 2003, 1399.
[13] G. Battistoni, hep-ph/0012268; Nucl. Phys. Proc. Suppl. 100 (2001) 101–106.
[14] G. Battistoni, A. Ferrari, T. Montaruli, P.R. Sala, Astropart. Phys. 17 (2002) 477.
[15] K. Abe et al., Phys. Lett. B 564 (8) (2003) 8;
T. Sanuki et al., Phys. Lett. B 541 (2002) 234, Erratum: Phys. Lett. B 581 (2004) 272;
M. Motoki et al., Astropart. Phys. 19 (2003) 113.
[16] J. Alcaraz et al., Phys. Lett. B 490 (27) (2000);
J. Alcaraz et al., Phys. Lett. B 494 (193) (2000).
[17] T. Sanuki et al., Astrophys. J. 545 (2000) 1135;
K. Abe et al., Phys. Lett. B 564 (2003) 8.
[18] M. Boezio et al., Astropart. Phys. 19 (2003) 583.
[19] G.D. Badhwar, P.M. O'Neill, Adv. Space Res. 17 (2) (1996) 7.
[20] G. Battistoni et al., Nucl. Phys. B, Proc. Suppl. 110 (2002) 336.
[21] M.G. Catanesi et al. (HARP Collaboration), CERN-SPSC/99-35, SPSC/P315; see http://harp.web.cern.ch/harp/.
[22] A. Mirizzi et al., Supernova Neutrino Physics with a Megaton detector, presented at Neutrino Oscillation Workshop (November 2004), 11–17 September 2004, Conca Specchiulla, Lecce, Italy.
[23] T.K. Gaisser, T. Stanev, G. Barr, Phys. Rev. D 38 (1988) 85.
[24] A.G. Cocco et al., JCAP 0412 (2004) 002, e-Print Archive: hep-ph/0408031.